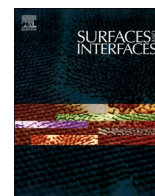




Since January 2020 Elsevier has created a COVID-19 resource centre with free information in English and Mandarin on the novel coronavirus COVID-19. The COVID-19 resource centre is hosted on Elsevier Connect, the company's public news and information website.

Elsevier hereby grants permission to make all its COVID-19-related research that is available on the COVID-19 resource centre - including this research content - immediately available in PubMed Central and other publicly funded repositories, such as the WHO COVID database with rights for unrestricted research re-use and analyses in any form or by any means with acknowledgement of the original source. These permissions are granted for free by Elsevier for as long as the COVID-19 resource centre remains active.



Impact of surface topography on the bacterial attachment to micro- and nano-patterned polymer films

Achille Francone^a, Santos Merino^{b,c,*}, Aritz Retolaza^b, Jorge Ramiro^b, Sofia A. Alves^b, Joana Vieira de Castro^d, Nuno M. Neves^d, Ainara Arana^e, Jose M. Marimon^e, Clivia M. Sotomayor Torres^{a,f}, Nikolaos Kehagias^{a,1}

^a CSIC and BIST, Catalan Institute of Nanoscience and Nanotechnology (ICN2), Campus UAB, Bellaterra, Barcelona 08193, Spain

^b Tekniker, Basque Research and Technology Alliance (BRTA), Eibar 20600, Spain

^c Departamento de Electricidad y Electrónica Universidad del País Vasco, UPV/EHU, Leioa 48940, Spain

^d 3B's Research Group, AvePark-Parque de Ciência e Tecnologia, Zona Industrial da Gandra, I3Bs-Research Institute of Biomaterials, Biodegradables and Biomimetics, University of Minho, Barco, Guimarães 4805-017, Portugal

^e Microbiology Department, Biodonostia Health Research Institute, Donostia University Hospital, San Sebastián 20014, Spain

^f Institució Catalana de Recerca i Estudis Avançats (ICREA), Barcelona 08010, Spain

ARTICLE INFO

Keywords:

Antibacterial
Nanoimprint lithography
Hierarchical surface topographies
Polypropylene films
Functional surfaces
Surface patterning

ABSTRACT

The development of antimicrobial surfaces has become a high priority in recent times. There are two ongoing worldwide health crises: the COVID-19 pandemic provoked by the SARS-CoV-2 virus and the antibiotic-resistant diseases provoked by bacteria resistant to antibiotic-based treatments. The need for antimicrobial surfaces against bacteria and virus is a common factor to both crises.

Most extended strategies to prevent bacterial associated infections rely on chemical based-approaches based on surface coatings or biocide encapsulated agents that release chemical agents. A critical limitation of these chemistry-based strategies is their limited effectiveness in time while grows the concerns about the long-term toxicity on human beings and environment pollution. An alternative strategy to prevent bacterial attachment consists in the introduction of physical modification to the surface. Pursuing this chemistry-independent strategy, we present a fabrication process of surface topographies [one-level (micro, nano) and hierarchical (micro+nano) structures] in polypropylene (PP) substrates and discuss how wettability, topography and patterns size influence on its antibacterial properties. Using nanoimprint lithography as patterning technique, we report as best results 82 and 86% reduction in the bacterial attachment of *E. coli* and *S. aureus* for hierarchically patterned samples compared to unpatterned reference surfaces. Furthermore, we benchmark the mechanical properties of the patterned PP surfaces against commercially available antimicrobial films and provide evidence for the patterned PP films to be suitable candidates for use as antibacterial functional surfaces in a hospital environment.

1. Introduction

We are currently living in a critical context since the World Health Organization (WHO) declared on 11 March 2020 the novel coronavirus (COVID-19) outbreak as a global pandemic. This announcement drove global attention to the tremendous social, financial and health impact that a virus (the SARS-CoV-2) is capable to unleash causing over 227.7 million infections and 4.6 million deaths worldwide so far [1]. In addition to the pandemic, there is another ongoing health crisis caused

by bacteria resistant to antibiotics. According to the report released by the United Nations Interagency Coordinating Group on Antimicrobial Resistance in 2019, if no action is taken, drug-resistant diseases could cause 10 million deaths worldwide each year by 2050 and by 2030, antimicrobial resistance could force up to 24 million people into extreme poverty [2]. Currently, at least 700,000 people in the world die each year as a result of drug-resistant diseases. These ongoing health crises are connected [3] considering that the widespread use of antimicrobial therapies, as part of the package of clinical care against COVID 19, could

* Corresponding author at: Surface Chemistry and Nanotechnologies Unit, Tekniker, Basque Research and Technology Alliance (BRTA), Eibar 20600, Spain.
E-mail address: santos.merino@tekniker.es (S. Merino).

¹ Present address: NCSR "Demokritos", Institute of Nanoscience & Nanotechnology, P. Grigoriou 27 & Neapoleos Str, 15341 Ag. Paraskevi, Athens, Greece.

increase the antimicrobial resistance related diseases. Although several measures have been put in place to manage this critical scenario, the WHO recently warned that the lack of new antibiotics threatens global efforts to contain drug-resistant infections [4].

Thus, the development of antimicrobial solutions and more concretely antibacterial solutions is an important and a high priority challenge and the ability to create passive antibacterial surfaces on different components has profound implications for human health services. Two main categories of solutions can be identified: those to be developed inside the human body (therapies) and those to be applied on external surfaces (prevention). Antibacterial solutions applied on surfaces reduce the attachment and proliferation of bacteria and they can be classified as antibiofouling (repel bacteria from attaching onto the surfaces) or bactericidal (inactivate the bacteria largely through chemical mechanisms or agents). Antibiofouling surfaces may prevent cellular attachment due to the presence of an unfavorable surface topography or surface chemistry against the microorganism and they can be based on surface coatings, but also surface chemistry modification (as are surface polarization, functionalization, and derivatization), or modification of the surface architecture of a substrate, considered a physical approach.

Chemical-based surface coatings with antibiofouling properties based on zwitterionic carboxy betaine coatings have been largely studied while silver, copper, quaternary ammonium compounds or antibiotics have been widely used as bactericidal coatings. However, the use of surface coatings as antibacterial agents has revealed several shortcomings. Bacteria can develop resistance against antibiotics and antibacterial agents [5], while the antibacterial agents can take a long time to be released from the surface and the concentration of the released agents may not be sufficient to maintain effective antibacterial properties. In parallel, chemical-based surface coatings have raised global concerns about what are the health and environmental impacts of the increased use of metallic nanoparticles and chemical-based coatings for antibacterial surfaces [6].

An alternative strategy to prevent bacteria-associated infections relies on a physical approach, introducing surface modifications at the micro and/or nano scale [7]. It consists in the development of antibiofouling engineered functional solutions capable to control the attachment of bacteria to a surface by the tuned degree of hydrophobicity and the pattern size in comparison to the bacteria, resulting in a chemistry-independent method with the added benefits of being a sustainable, safe and nature-inspired strategy. Among the first studies based on this approach, Ivanova et al. demonstrated that bio-inspired patterns, such as those of the cicada [8] and dragonfly wings [9], have an additional effective bactericidal behavior. Antibiofouling properties based on the topographical-physical based approach have been largely studied but the relative importance of wettability and surface topography remains to be elucidated [10]. In some cases, smaller surface features are more effective at reducing bacterial retention, as the preferential alignment of bacteria to valley and pillar structures demonstrates that cells seek to maximize contact area for improved attachment [11]. On the other hand, hydrophobicity has been largely attributed to generate antibiofouling surfaces [12], even though both superhydrophilic and superhydrophobic surfaces with the same topography have showed to create regions of preferential attachment for specific cell types [13] as well as higher hydrophobic surfaces with the same topography have showed higher antibiofouling properties for *Micromonospora purpurea* adhesion [14]. Apart from it, antibiofouling properties of highly hydrophobic surfaces have been justified due to an entrapped air-bubble layer that reduces contact between the bacteria and surface while this capacity is lost under prolonged immersion in water, potentially losing their antibiofouling properties [15].

Several patterning techniques can be employed to fabricate these micro and nano structured surfaces [16] including lithography-based ones, reactive ion etching (RIE) and femtosecond laser writing, among others. Nanoimprint lithography (NIL) [17] is a suitable candidate to

realize bioinspired patterns, as it is a high-resolution lithographic method with generally low cost, high throughput and the ability to use different substrates materials, allowing surface structuring of transparent and flexible materials [18]. Several examples of bio-inspired topographies fabricated by batch-to-batch NIL can be found in the literature based on one-level nanocones [19], nanopillars [20–24], micro lines [25] and micro mushrooms [26]. Using NIL is possible to fabricate multi-scale topographies combining micro- and nano-structures, denoted as hierarchical structures [27–33]. Recently, Alameda et al. [34] employed several steps of photolithography and NIL to fabricate hierarchical structures on different substrates, showing how these topographies exhibit a superhydrophobic behavior. Psocchia et al. [35] have recently fabricated hierarchical structures on PLLA composite films with enhanced antibacterial properties for smart packaging applications.

Here we have designed and fabricated hierarchical topographies combining the introduction of physical features smaller and larger than the bacteria size on the same substrate while providing an almost superhydrophobic behavior. These structures have been compared in terms of antibiofouling properties with morphologies based solely on smaller or larger features than the bacteria size on the same type of substrate, providing a different wettability behavior. We have chosen a cheap and commercially available flexible substrate (Polypropylene, PP), without biochemically modifying the material composition [36] and without the need of applying additional surface chemical treatments. We study the influence of wettability and hierarchical topography on the bacteria adhesion, while reporting a potentially industrial scalable manufacturing process with NIL patterned surfaces consisting of various topographies, one-level (micro, nano) and hierarchical (micro- and nano) structures. The hierarchical structures were designed following the principles of Cassie-Baxter and Wenzel wettability models [37–39], while thermal NIL was used as patterning technique. We show a distinct bacterial attachment of Gram-negative *Escherichia coli* and Gram-positive *Staphylococcus aureus* bacteria in unpatterned and patterned samples, while the hierarchical surfaces present a superior resistance to bacterial attachment as compared to one-level patterning comprised of micro or nanofeatures. Furthermore, benchmarking of the patterned PP substrates with respect to physical (topography and wettability) and mechanical properties (tensile and tear strength, resistance to wear under wet assays) was carried out in a comparison to other commercially available antimicrobial films. Additionally, the patterned films were characterized over time as treated with a cleaning protocol usually followed in hospitals environments, including disinfectants and regular cleanings mimicking the natural environment in which these surfaces usually work.

2. Experimental details

2.1. Materials and silicon master stamps fabrication

PP substrates with a thickness of 100 μm were provided by the film supplier Propagroup S.p.A. (Italy). Different topographies containing one-level and two-levels topography features, in the micro- and nanometer scale, were designed and fabricated. Silicon master stamps, realized by established silicon technologies, were used in the thermal NIL process. Initially, one-level masters containing black silicon-like features (nanospikes) were fabricated using a reactive ion etching (RIE) process (Plasmalab 80+, Oxford Instruments) on a 100 mm silicon wafer. The RIE conditions were: pressure = 80 mTorr, power = 50 W, SF_6/O_2 flow ratio = 32/24 sccm, etch time = 3000 s. The obtained black silicon nano topographies presented an average height of 2.2 μm and a base diameter of 300 nm. For the one-level micro scale topographies, a combination of photolithography and RIE techniques were used to realize two-dimensional (2D) micropillar array structures. A quartz photolithography mask was used to create positive features within a 10 μm thick AZ 2035 nLoF photoresist spin coated on a 100 mm silicon wafer. After

photolithography, the unexposed areas of the photoresist were developed, followed by a RIE step to transfer the pattern to the underlying silicon substrate. The Bosch process was used to achieve 10 μm high in height micropillar structures. The conditions of the ICP-RIE process were: SF_6 flow = 172 sccm with cycle time = 6 s, C_4F_8 flow = 110 sccm with cycle time = 3 s, power = 1800 W, bias voltage = 60 V, pressure = 37 mTorr and wafer temperature = 15 $^\circ\text{C}$. Two-level topographies, containing both micro and nano scale structures, were realized by using a combination of the above two techniques, first patterning the micropillar arrays and subsequently the nanospikes.

2.2. Design of antibacterial topographies

The design strategy of antibacterial surfaces was based on creating highly hydrophobic patterned surfaces with a higher as possible contact angle. The first level (micro pillars) topographies of the hierarchical structures were designed based on the Cassie-Baxter and Wenzel state models [38,39], where high roughness factor and small solid-liquid contact fraction are needed to get superhydrophobic surfaces. Squared arrays of micropillars with cylindrical shape were analyzed as microstructure-level structure corresponding to a roughness factor and solid-liquid fraction defined as follows (Eqs. (1) and (2)):

$$r = 1 + \frac{dh}{a^2} \quad (1)$$

$$f_{SL} = \frac{\pi}{4} \left(\frac{d}{a}\right)^2 \quad (2)$$

with d , h and a representing the pillar diameter, height and period, respectively. A low f_{SL} and a high r compatible with the fabrication protocol was chosen. Taking into account that, micropillar depths above 10 μm led to an inhomogeneous density of the second level topography (nanospikes), 10 μm pillars height was selected. On the other hand, as the size and the space between the pillars is increased, the Cassie-Baxter state will become more unstable because of the larger meniscus penetration. Therefore, it would be easier for the droplet to move into the Wenzel state. As a consequence, micropillars diameters of 4 and 10 μm and periods of 11 and 23 μm respectively were selected not showing differences between them in a preliminary assessment of the antimicrobial trials (data not shown). Pillars with 23 μm pitch and 10 μm diameter were finally selected due to its ease for fabrication. These geometrical dimensions lead to a calculated roughness factor of 1.59 while the solid-liquid contact fraction is 0.14.

The addition of the nanospikes to the micropillars has two different functions: to increase the surface roughness and to decrease the solid-liquid contact fraction. For a hierarchical micro nanostructure, the f_{SL} is calculated by multiplying the area fraction of the microstructure and the area fraction of the nanostructure and therefore the f_{SL} of a two-level structure in contact with a liquid is much smaller than that of a single-level structure. In the case of nanospikes, the random distribution of the structures, make difficult calculating the f_{SL} .

2.3. Fabrication of working stamps

Although in this work we present only results related to PP samples that were patterned using NIL in batch-to-batch mode, we targeted the development of an industrially scalable manufacturing process, based on the continuous patterning of antibacterial flexibles PP films through NIL (thermal roll-to-roll NIL), where the fabrication of nickel stamps (named "working stamps") is required. Therefore, the silicon master stamps were copied into nickel working stamps using an electroforming process. The silicon master stamps were coated with a conductive metallic thin layer. First, a thin layer of titanium (< 10 nm), which acts as an adhesive layer, was deposited using physics vapor deposition. Subsequently, a thin layer of copper (< 10 nm), which acts as a seed layer, was deposited

using an electron beam evaporation system (ATC-Orion-8E UHV, from AJA Int.). The coated substrates were then immersed in a nickel sulphamate solution. Typical composition and operating conditions were: nickel sulphamate [$\text{Ni}(\text{NH}_2\text{SO}_3)_2 \cdot 4\text{H}_2\text{O}$] = 300–450 g/L, nickel chloride ($\text{NiCl}_2 \cdot 6\text{H}_2\text{O}$) = 0–30 g/L, boric acid (H_3BO_3) = 30 g/L, temperature = 40–60 $^\circ\text{C}$, pH = 3.5–4.5, cathode current density = 2–15 A/dm², deposition rate = 25–180 $\mu\text{m}/\text{h}$. During electroplating the pH was adjusted to 3.8–4.2 using a pH correcting solution, based on boric acid at a constant temperature of 50 $^\circ\text{C}$. The rate of deposition was controlled by the current applied to the electroplating plant ($\mu\text{-Galv}$ MOT Semi-con). During nanospikes replication, a low current ($I = 0.05$ A) was used to maintain an approximate electrodeposition rate of 1 $\mu\text{m}/\text{h}$, while in the case of micropillars topographies the current was increased to achieve an electrodeposition rate of 10 $\mu\text{m}/\text{h}$. In both cases, in the last step of the electroforming process, the deposition rate was reduced to 1 $\mu\text{m}/\text{h}$ to obtain a good finishing quality also in the rear part of the stamp. After the electrodeposition process, the silicon substrates were etched using a KOH aqueous solution (30% in weight). The solution was heated at 80 $^\circ\text{C}$, resulting in an etching rate of 1.1 $\mu\text{m}/\text{min}$, without etching neither copper nor nickel. Once all the silicon had been etched, the remaining copper was removed using a copper etchant (Transene copper etchant 49:1). Finally, in order to prevent possible adhesion issues during the imprinting process, the nickel working stamps were treated using Perfluoro-octanephosphonate (PFOP) as an anti-adhesion treatment (Sigma-Aldrich). The nickel stamp was cleaned regularly (each 10–12 imprinting cycles) with xylene solvent (Sigma-Aldrich) to dissolve any polypropylene debris left during the imprinting cycle while acetone and isopropyl alcohol were used afterwards for rinsing. The nickel stamp was used at least 80 times without any damage of the patterned surface.

2.4. Fabrication of patterned PP substrates by nanoimprint lithography

The 100 μm thick PP substrates were patterned by thermal nanoimprint lithography in batch-to-batch mode using the nickel working stamps and a desktop CNI tool from NIL Technology ApS. The patterned surface was 90 mm in diameter and imprinting conditions were optimized to 180–210 $^\circ\text{C}$ temperature, 3–5 bar pressure for 3–6 min and 40–60 $^\circ\text{C}$ separation temperature.

2.5. Morphological assessment

The quality of the topographical features was assessed by SEM characterization using, respectively the field emission scanning electron microscopy (FE-SEM) Zeiss Ultra Plus and the FEI Quanta 650 FEG.

2.6. Antimicrobial assessment

The antimicrobial properties of the patterned PP surfaces were evaluated following the touch transfer assay method [40], optimized after a consistent comparison with other standard methods. The touch transfer assay assesses the attachment and survival of the remaining viable bacteria directly on the surface of films with the help of a velvet pad previously immersed in the bacterial suspension, thus overcoming the difficulty in spreading the inoculum of bacteria in very hydrophobic surfaces. It also allows replicating the contamination of a film surface when touched by many users for a short time eventually carrying bacteria.

2.7. Cytocompatibility assessment

The cytocompatibility of the patterned PP surfaces was evaluated by the MTS assay, where the films were cut into 0.6 cm diameter circles and were fixed with previously sterilized carbon adhesive tape at the bottom of wells of 96 multi-well plates. The L929 cell line was used in those experiments. 3×10^3 L929 cells were seeded on the patterned and on the unpatterned films in triplicate, in DMEM low glucose (Gibco)

containing 10% foetal bovine serum (FBS, Gibco) and 1% antibiotic-antimycotic solution (Gibco). Cells were incubated in a humidified atmosphere at 37 °C and 5% (v/v) CO₂. After 1, 3, or 7 days in culture, the viability of L929 cells was evaluated using CellTiter 96® Aqueous One Solution Cell Proliferation Assay (MTS, Promega). At each time point, the cells were exposed to the medium containing MTS in a 5:1 ratio for 3 h in a humidified atmosphere at 37 °C and 5% CO₂, while the optical density (O.D.) was determined at 490 nm. The cells' viability was calculated, in the case of the two types of hierarchical topographies, in accordance with Eq. (3):

$$\% \text{ Cell viability} = \frac{O.D. \text{ patterned}}{O.D. \text{ unpatterned}} \times 100 \quad (3)$$

2.8. Mechanical properties and wettability

Physical (wettability) and mechanical properties (tensile and tear strength, resistance to wear under wet conditions) of the hierarchically patterned PP substrates (later referred in the text as Micro/nano patterned PP) were benchmarked against commercially available products.

Regarding the wettability, contact angles of distilled water in contact with materials surface were measured with a SURFTENS universal goniometer. For these measurements, a droplet of approximately 4 µL of distilled water was gently manually dispensed on the surface of the tested materials with the help of a syringe and the angle was measured immediately after the drop was delivered on the surface, illuminating with diffuse light to obtain a sharp image of the drop border. The contact angle hysteresis was calculated by measuring the advancing and receding angle. The advancing angle is determined by measuring the angle observed as an additional 5 µL droplet is added, while the receding angle is measured as this 5 µL droplet is extracted. The difference between these two angles is the contact angle hysteresis. The image is recorded with a camera and the angle between the baseline of the drop and the tangent at the droplet boundary is measured by adequate software. The error of the acquisition of the camera is 0.5°. All tests were made at a temperature of 21 ± 2 °C and a relative humidity of 41 ± 3%.

Regarding the mechanical properties, tensile tests were performed following the UNE-EN ISO 527-3. For these tests, a universal testing machine (Instron 3369 model) was used. The cell was of 1 kN capacity and pneumatic clamping system was employed to hold the samples. The test velocity was 5 mm/min. The specimen dimensions were adapted for this test and reduced proportionally to the overall length, which instead of 152 mm was set as 90 mm, due to the dimensions of the stamps used for structuring the polymer films by NIL. The samples were extracted from the base materials with a die cutter designed specifically with the shape of the specimens desired. A minimum of five independent tests were carried out for each material.

The trouser tear strength of the reference and micro/nano patterned PP films was determined by tear strength tests following ISO 34-1 and ISO 6133 international standards. This is defined as the median force required to propagate a cut in a specified trouser-shaped test piece by tearing, divided by the thickness of the test piece. A minimum of five independent tests were carried out for each material.

Washability tests were carried out to assess the resistance to wear under wet conditions using a wet-scrub tester (Neurtek). The physical and chemical agents used for this test were provided by the Donostia University Hospital (HUD), to better mimic the real cleaning procedure followed in a hospital environment. A cleaning cloth typically used in HUD for bedroom cleaning served as the physical agent and the disinfectant NEUTROSOL BRISA (containing bio-alcohol: 5-chloro-2-methyl-2,3-dihydrothiazol-3-one, 2.5 v/v%) was used as the chemical one. These tests were carried out at a frequency of 37 ± 2 cycles/min (UNE-EN ISO 11998), for 810 cycles (mimicking, in triplicate, the 30 washings of 1 month, for a total of 9 months) and an estimated contact pressure of 1.6 kPa was applied during the reciprocating movements mimicking

daily cleaning actions. All films were characterized before and after the washability tests regarding their brightness and wettability to evaluate how cleaning activities may influence the features of these films.

3. Results and discussion

3.1. Morphology control and wettability of hierarchical surfaces

Although in this work we present only results related to PP samples that were patterned using NIL in batch-to-batch mode, we targeted the development of an industrially scalable manufacturing process, based on the continuous patterning of antibacterial flexible PP films through NIL (thermal roll-to-roll NIL), where the fabrication of nickel stamps (named "working stamps") is required. Therefore, the topographies contained in the silicon master stamps were first copied into nickel working stamps (using an electroforming process), then replicated into 100 µm thick PP substrates (using batch-to-batch thermal NIL). The selected topographies to evaluate their influence on the bacteria (*E. coli* and *S. aureus*, which present dissimilar geometry [rod cylinder shape and round shape, respectively] and similar dimensions [1-2 µm long by 1 µm diameter and 0.5-1 µm diameter, respectively]) adhesion were: (a) one-level micro (pillars with 10 µm diameter, 23 µm pitch and 10 µm height) and one-level nano (spikes with an average height of 2.2 µm and a base diameter of 300 nm) structures, representing both larger and smaller features than the targeted bacteria; (b) hierarchical (combination of micro-and-nano) structures aiming to provide high hydrophobicity, presenting nanostructures at the bottom of the micropillars in a configuration and nanostructures on top in the other one.

The morphology of the topographies under study was characterized by scanning electron microscope (SEM), as shown in Fig. 1.

Inspection of the SEM micrographs showed that the density of nanostructures had an impact on the replication quality in the PP substrate. In particular, for the one-level topography which contained nanospikes structures, it appeared that the nickel stamp induced a pulling effect which resulted in spaghetti-like PP features. The observed pulling effect is explained as the result of the high contact area between the nickel stamp and the PP substrate during the separation step in the nanoimprint lithography process. The same effect was observed in the case of the hierarchical topography with nanostructures at the bottom part of the micro patterned substrate. In the case of the hierarchical topography with nanostructures on the elevated parts of the micropillars, the contact area between stamp/substrate is smaller than in the previous cases, resulting in weaker separating forces providing standing nanospikes. The imprinting of nanostructures at the top and at the bottom of micropillars was not possible because the demolding force deformed completely the features.

Static water contact angle (WCA), hysteresis contact angle (HCA) and sliding angle were determined for hierarchical patterned PP surfaces (see Table 1). Both types of topographies present a WCA value well above 100° (while for the unpatterned PP film, one-layer microstructures and one-layer nanostructures, it resulted to be 97.8 ± 1.1°, 117.2 ± 1.5°, and 106.2 ± 1.5°, respectively), which can be defined as highly hydrophobic. In the case of the nanostructures on the upper part of the pillars the WCA is very close to 150° and is higher than the configuration with nanostructures at the bottom (≈147° and ≈133°, respectively) because the nanospikes hold a higher volume of air trapped in-between the features, which helps to reduce the contact area between the solid substrate and the drop (resulting in a higher WCA). Furthermore, the HCA values were well below 15° (≈2° and ≈6°, respectively), indicating that the water drop had a low adhesion to these patterned surfaces. This is of utmost importance since this feature may influence the ability of bacteria to adhere to the surface and proliferate, and therefore impact the antimicrobial behavior of the film. The hierarchically patterned PP substrates can be therefore defined as highly hydrophobic and represent an excellent result considering that their wetting behavior was achieved without the use of any chemical coating, chemical treatment or material

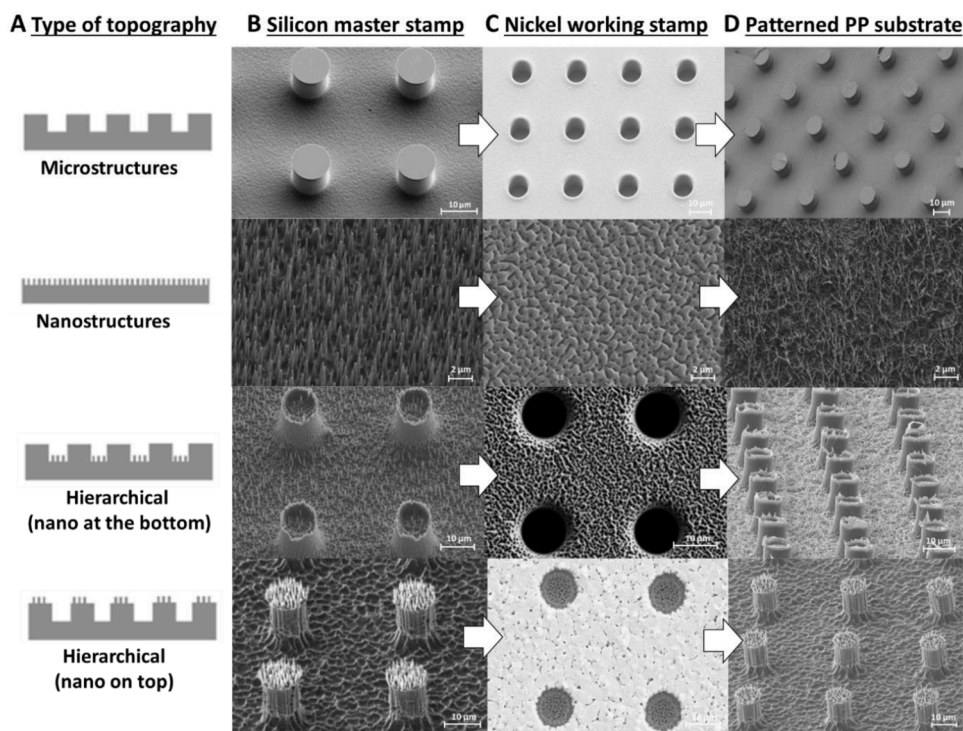
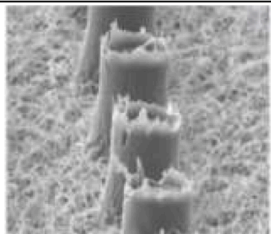

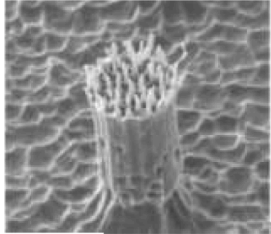



Fig. 1. (a) Schematics for the selected topographies and (b–d) SEM images showing their aspect after the fabrication of the silicon master stamps (b), the nickel stamps (c) and the patterned PP substrates (d).

Table 1

Wettability measurements for the hierarchical topographies: static water contact angle, hysteresis and sliding contact angle.

Topography	Contact angle [°]		
	Static	Hysteresis	Sliding
Hierarchical (nano at the bottom) 	 133.4±0.5	5.8±2.5	Pinning
Hierarchical (nano on top) 	 146.9±0.5	1.8±0.7	15.6±2.8

modification. Furthermore, the sliding angle was also studied for both types of samples: in the case of the hierarchical one with nanostructures at the bottom, the drops of water stayed pinned to the surface (with no sliding), while in the hierarchical one with nanostructures on top a sliding angle of about 15° was measured.

3.2. Physical characterization of the patterned films

The topographical-based PP films were analyzed in terms of mechanical properties, gloss and hydrophobicity and compared to the following antimicrobial commercial films references: (a) a 70 μm thick

FLEXcon® Sharklet™ (Flexcon) [41], which is claimed to be an inhibitor of microbial attachment due to its topography (patterned polyvinyl chloride lines with about 3 μm height, 2 μm width and variable length between 2 and 10 μm, mimicking the texture of shark skin); (b) a 160 μm thick Autotex® AM (MacDermid) [42] (hard coated PET film incorporating Microban® protection based on silver ions, polyhexanide, quaternary silane or zinc) and (c) a 80 μm thick Pure Zone® (Hexis) [43] (PVC film based on silver ions and triclosan), where (b) and (c) incorporate chemical agents which bestow them antimicrobial properties by killing bacteria.

Data shown in Figs. 2 and 3 correspond to the topography presenting

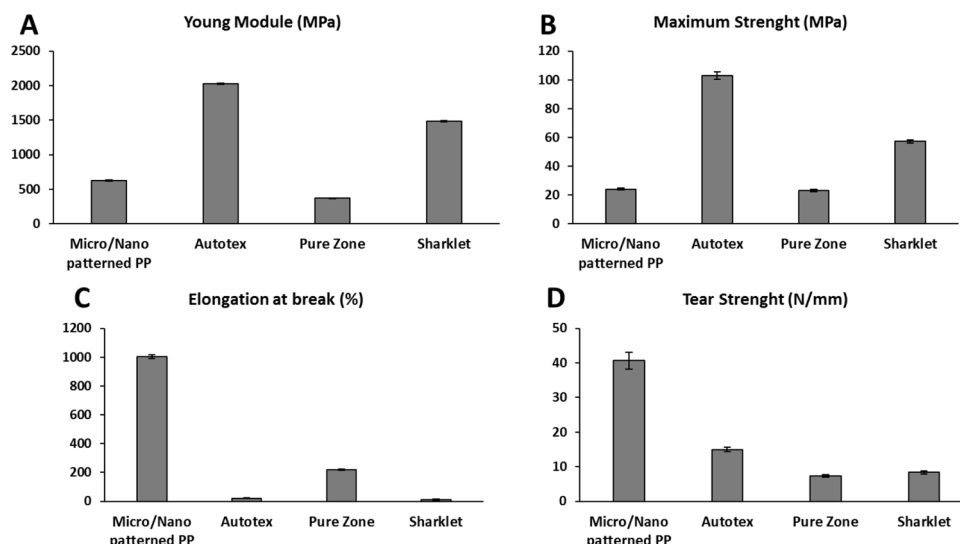


Fig. 2. (a) Young module, (b) maximum strength, (c) elongation at break, (d) tear strength of the micro/nano patterned films and commercial products.

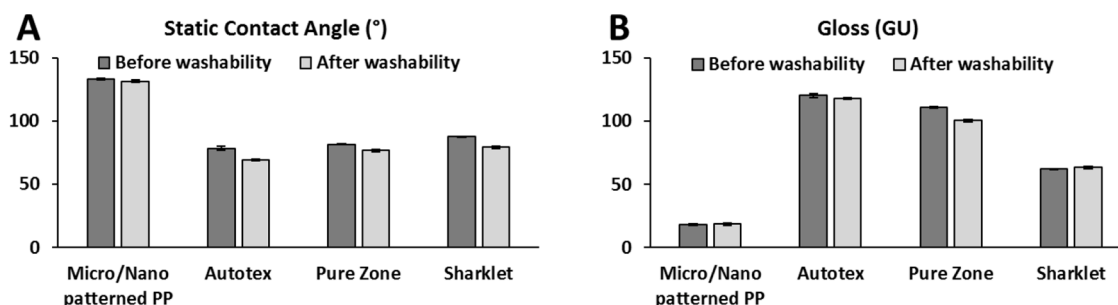


Fig. 3. (a) Variation of the static contact angle and (b) gloss after the washability tests for the patterned film and commercial references. Data are presented as the mean \pm SD of independent experiments.

nanospikes at the bottom of the micropillars since no differences were found between neither both type of hierarchical topographies nor for the topographies called microstructures and nanostructures, except for the WCA (as mentioned above). It is also noted that mechanical properties of the blank PP film do not change after the replication of any of the four different topographies onto the film surface.

The mechanical tensile properties of micro/nano patterned films and commercial references were assessed by determining their Young's modulus, maximum strength and elongation at break point, and the results obtained are summarized in Fig. 2(a)–(c). The Autotex film displays the highest Young's modulus and maximum strength followed by the Sharklet and Pure Zone films. This last one displays a significant higher elongation at break compared to Autotex and Sharklet films. By comparing the results obtained between the micro/nano structured PP film and the commercial films, it is observed that the Young's modulus and maximum strength values determined for the fabricated film, although lower than those measured for Autotex and Sharklet, are similar to those of Pure Zone film. On the other hand, the PP textured film displays a significant higher elongation at break point, suggesting a more flexible behavior as they can deform considerably before breaking.

The resistance to tearing of the micro/nano patterned film was also determined and compared to the commercial references, as illustrated in Fig. 2(d). It must be stated that this film shows a significantly higher resistance to tearing as compared to all the commercial references. This superior tear strength is considered relevant as the film should be exposed to tearing forces when in use at application sites.

Washability tests were performed with a specific cleaning protocol usually followed in hospitals environments, mimicking the natural

environment in which these surfaces usually work. Considering the results after the washability tests shown in Fig. 3, it is observed that the cleaning procedure does not significantly affect neither the gloss nor the WCA of the films. It is important to note that both WCA and gloss kept unaltered after the washability tests for each type of the four topographies studied.

For the commercial references there is no change in gloss after washability tests, except for Pure Zone, which shows a slight reduction in brightness. Based on gloss measurements, the different films may be classified as matt, mid gloss or bright. Sharklet is mid gloss while Autotex AM and Pure Zone are bright (before and after washability tests). The micro/nano patterned PP films showed a gloss value between 15 and 20 GU before and after washability tests and therefore can be classified as mid gloss surfaces, with a lower brightness compared to all commercial references in this work. Regarding WCA measurements, there is a trend for Autotex AM to display a lower WCA compared to Sharklet and Pure Zone. The micro/nano patterned PP films exhibited a WCA of about 130° before and after washability tests, while the topography is unaffected by the cleaning protocol, highlighting their stronger hydrophobic nature compared to the commercial references before and after cleaning activities.

Following this analysis, the PP micro/nanopatterned film shows a behavior, in terms of mechanical properties and resistance to the cleaning protocol, suitable to be used in real hospital environments.

3.3. Cytocompatibility of the patterned films

The results of the cytocompatibility assays of patterned films, which

were obtained following the MTS assay, are illustrated in Fig. 4 and show that the presence of topography on the patterned PP substrates does not decrease the metabolic activity of L929 cells when compared to unpatterned films. This means that the patterned PP substrates are cytocompatible.

The unpatterned films were used as positive control of the cytocompatibility in those experiments. The results show that after 1 day the metabolic activity of cells seeded in patterned films is comparable to those cultured in unpatterned films, being lower in the hierarchical pattern with nanopikes at the top. This lower metabolic activity may be caused by the higher hydrophobicity of those films (bordering superhydrophobicity) that hinder the seeding and attachment of the cells. After 3 days of culture, the metabolic activity of cells cultured in the patterned films is lower than that of cells cultured in unpatterned surfaces, even in the absence of statistically significant differences. This may still be related to the difficulty of cells to spread and proliferate due to the very high hydrophobicity of the patterned films. After 7 days of culture, the cells recover the level of metabolic activity in the patterned films. Moreover, in the patterned films with nanopikes at the bottom, the metabolic activity of the cells is higher (with statistically significant differences, $p = 0.004$) than that of the unpatterned films. Those results show that the patterned PP substrates are cytocompatible for the cells.

3.4. Antimicrobial performance of the patterned films

The antimicrobial behavior of the topographical-based PP films was studied using the touch transfer assay method [40]. Firstly, one-level patterned and unpatterned PP films were tested with Gram-negative *E. coli* and Gram-positive *S. aureus* bacteria, as shown in Fig. 5, at time-point 0 min (characterizing the attachment of the bacteria to the films and its short-term survival). A reduction of 46.2% for the *S. aureus* attachment was observed in the film with micropillars, from 132 ± 34 to 71 ± 49 CFU per plate ($p = 0.0012$), together with a pronounced standard deviation in the data. The same type of patterned film presented a lower reduction, only 21.4% (from 117 ± 42 to 92 ± 55 CFU, $p = 0.5654$) with *E. coli*. For the film with only nanostructures (black silicon) no reduction was observed in *E. coli* (112 ± 48 CFU per plate, $p = 0.8014$) nor in *S. aureus* (142 ± 16 , $p = 0.2296$).

These results indicate that the selected one-level topographies are not efficient in avoiding the attachment of *E. coli* nor *S. aureus*. According to these data, neither features larger nor smaller than the bacteria size have a relevant outcome in the bacteria attachment for a similar behavior of wettability. Moreover, features larger than bacteria size show slightly antibiofouling properties, especially for *S. aureus*. In order to confirm the efficacy of our strategy, we studied the behavior of both hierarchical topographies at time-point 0 min with the same type of bacteria, as shown in Fig. 6. A significant reduction of the *E. coli* and *S. aureus* attachment was observed in the film with nanostructures at the

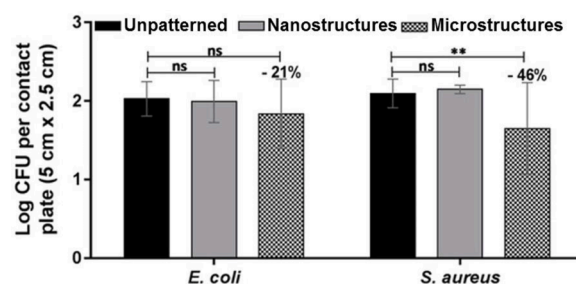


Fig. 5. Quantification of the antimicrobial performance of patterned PP surfaces against *E. coli* and *S. aureus* according to touch transfer assay at time-point 0 min. Data are represented as the CFU mean \pm SD of three independent experiments (** $p \leq 0.01$).

bottom of the micropillars: 82% reduction in *E. coli*, from 250 ± 116 CFU per plate to 45 ± 53 CFU per plate ($p = 0.0028$) and 84.2% reduction in *S. aureus*, from 273 ± 118 CFU per plate to 43 ± 32 CFU per plate ($p = 0.0010$). In the film patterned with nanostructures on the micropillars, a 86.3% reduction in the attachment was observed for *S. aureus*: from 182 ± 132 CFU per plate to 25 ± 25 CFU per plate ($p = 0.0169$). However, this reduction in the attachment was less significant for *E. coli*: 44.1% reduction, from 211 ± 81 CFU per plate to 118 ± 81 CFU per plate ($p = 0.1558$). The method used for measuring antimicrobial activity was based on bacterial culture, which gave high SD. Other non-culturing methods for determining bacterial load have been used, as luminescent quantification of bacterial ATP level (BacTiter-Glo™ Microbial Cell Viability Assay, Promega), a colorimetric assay based on the reduction of a tetrazolium salt by bacterial dehydrogenases (WST-1 test, Merck) [44], microplate laser nephelometry or fluorescence bacterial staining among others [45]. However, these methods, probably more accurate than bacterial culture, are based on different bacterial properties and hence, vary significantly in their outcomes [46,47] and many of them do not show the viability of the bacteria present on the surfaces.

These results demonstrate that the presence of nanopikes at the bottom of the micropillars is more effective since it inhibits the attachment of Gram-negative and -positive bacteria while the nanopikes on the micropillars are only effective against the Gram-positive *S. aureus*. Furthermore, the nanopikes were efficient only when placed at the bottom of a hierarchical topography but not when they are placed at the bottom in a one-layer configuration, as shown in Fig. 7. In fact, looking at the pictures of petri-dishes half covered with unpatterned PP films and half with patterned ones, it is clear and visible the effect played by the topography. When the topography corresponds to one-level nanostructures, the petri-dishes do not show any difference in bacterial attachment between the patterned and the unpatterned side (b), both for *S. aureus* and *E. coli*. In the case of the hierarchical structure with

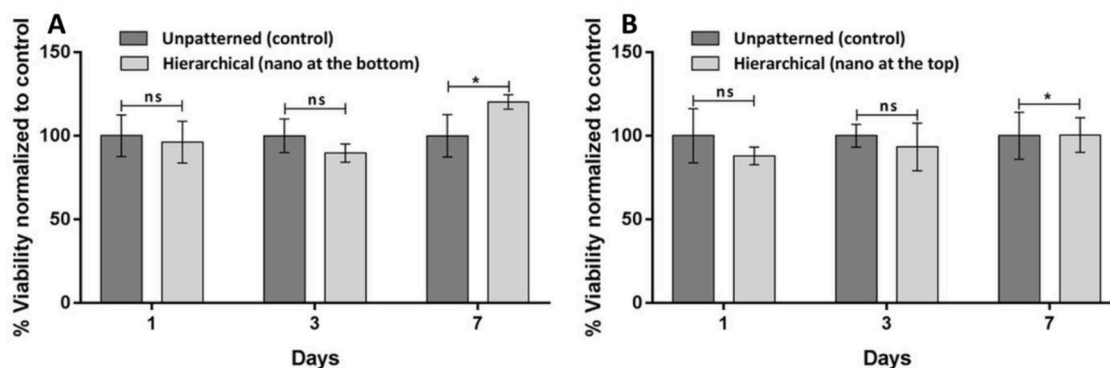


Fig. 4. Cytotoxic effect of films patterned with hierarchical structures: (a) nanopikes at the bottom and (b) nanopikes on top. Data is represented as the mean \pm SD of three independent experiments (* $p \leq 0.05$).

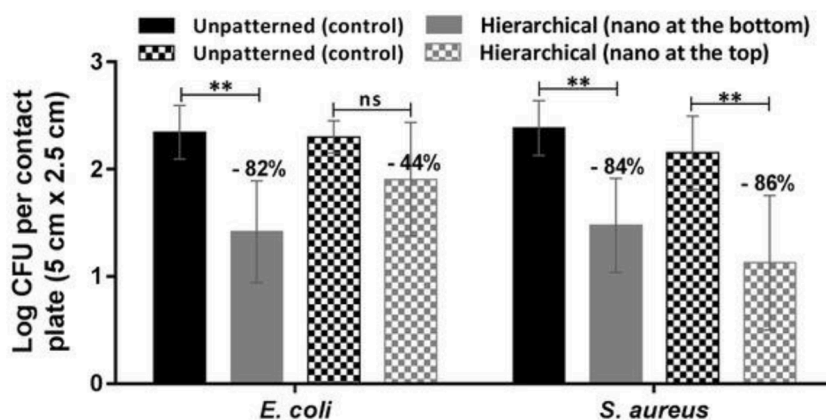


Fig. 6. Antimicrobial behavior of *E. coli* and *S. aureus* in hierarchically patterned and unpatterned PP films using the touch-transfer method at time-point 0 min. Data are represented as the mean \pm SD of three independent experiments (** $p \leq 0.01$).

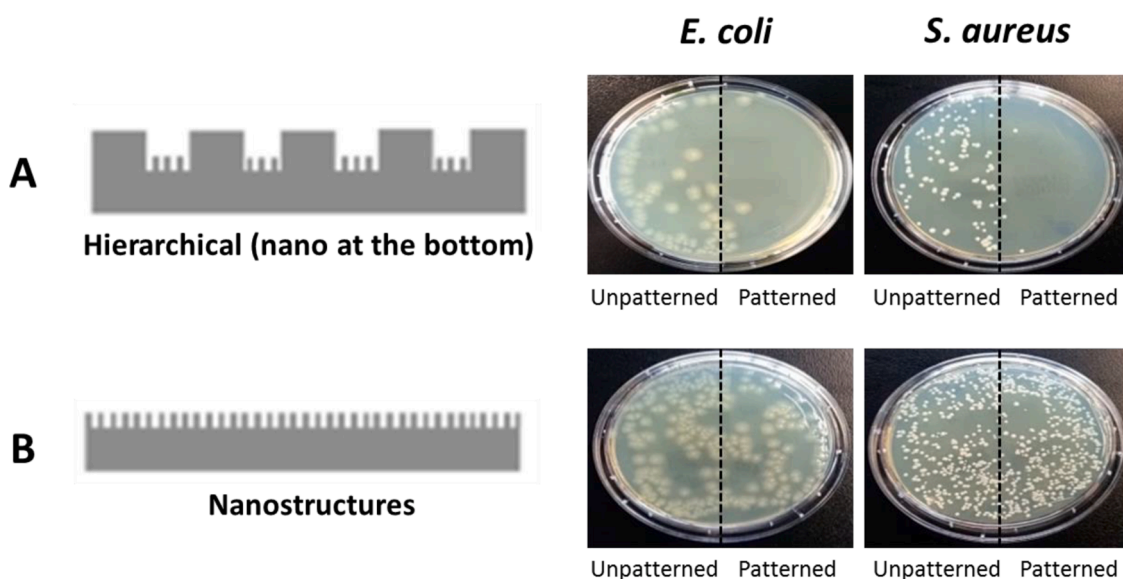


Fig. 7. Impact of nanostructures on the antimicrobial behavior of PP films (placed in petri-dishes) when fabricated in the hierarchical topography at the bottom (a) and in the one-level one (b) at time-point 0 min. Each petri-dish is half covered with an unpatterned film and half with a patterned one, showing, respectively remarkable (a) or no (b) differences.

nanostructures at the bottom (a), a clearly visible change appears in the patterned side, with almost no *E. coli* nor *S. aureus* bacteria appearing.

We have demonstrated that hierarchical structures provide a reduction in the attachment of bacteria to the surfaces. Considering the results in Fig. 7 and relating them to those in Table 1, it appears that the water contact angle plays a role to predict the capacity of the bacteria to attach onto the surface but alone it is insufficient to predict bacteria attachment. Our results are in agreement with previous studies [48,49], in which wettability of the surface does not correlate with cellular attachment across diverse materials. It means that the bacteria-surface interaction cannot be only described by an interaction between two surfaces of different surface energies, but the bacteria interact with the surface in a dynamic way, using different mechanisms to attach rather than behaving as an inert system. In fact, the ability of the bacterial cell to remain attached to a surface reflects the nature of non-covalent interactions between the substrate and cell wall functional groups during the initial phase of the attachment. The bacteria response is governed by its genome, in which many genes are devoted to environmental sensing and adaptation [50]. It is translated in surface sensing via surface appendages such as flagella and membrane associated sensor proteins. Considering the experimental data, in which hierarchical features with

nanospikes at the bottom are more effective to avoid the *E. coli* binding onto the surface, the dominance of surface morphology over wettability is evident, with water repellence playing a limited role while antibacterial performance is clearly showed. This finding is consistent with other references studying interaction of *E. coli* with stainless steel surfaces micro/nano textured by laser [49,51]. The response of *S. aureus* appears to be more influenced by wettability. In this case, the almost super-hydrophobic surfaces provide certain improvements over control samples and hydrophobic surfaces, in agreement with previous studies [51].

On the other hand, topographical features as those studied here, are supposed to be more effective to avoid bacteria attachment as the feature size is smaller than the bacteria size [52], avoiding higher attachment strength associated to the large available contact area [53]. Following this reasoning, in the present study, *E. coli* and *S. aureus*, chosen to represent Gram-negative and Gram-positive bacteria strains, respectively, with dissimilar geometry, are shown to exhibit very different responses due to its different surface sensing and shape (rod-cylinder shape and round shape, respectively) while they have similar critical dimensions (1-2 μm long by 1 μm diameter and 0.5-1 μm diameter, respectively). Thus, a rod-shape *E. coli* seems to have more

difficulties to attach to a high roughness surface like the one comprised by high density spikes (around $10^6/\text{mm}^2$) at the bottom ($13\ \mu\text{m}$ space between pillars) rather than to a much lower density of spikes placed on the micropillars ($10\ \mu\text{m}$ diameter). Conversely, a round-shape *S. aureus* do not show preferences to adhere to any of the hierarchical features. Moreover, the introduction of smaller features sizes compared to bacteria size cannot solely explain the antibiofouling properties of the surface (Fig. 5). The bacterial surface of Gram-positive and Gram-negative bacteria are different in composition, having Gram-negative bacteria a layer of lipopolysaccharide at the external surface, while the main cell wall component in Gram-positive bacteria is a thick layer of peptidoglycan [54]. Although minor variations could be expected in the antimicrobial activity of different surfaces with other bacterial species, big variations are not expected as *S. aureus* and *E. coli* are in general good representatives of the bacterial surface of Gram-positive and Gram-negative bacteria (in terms of sizes, shapes and cell envelope), respectively.

Here, it is relevant to mention not only the difference in the nanospikes density for both hierarchical topographies, but also the difference in their aspect after the demolding step in the NIL process. In fact, they appear folded and stretched when fabricated at the bottom of the micropillars, due to higher demolding forces associated to the higher density of the spikes, while standing and regularly distributed when placed at the top. It is also noteworthy that when the topography is extended to large surfaces is important to get well replicated micropillars over the whole surface area of the polymer avoiding slight deformation of them as observed in this work because of the demolding forces. This is particularly relevant as the fabrication process is extended to a continuous mode by roll-to-roll imprint of high roughness surfaces. Thus, minimization of demolding forces is an important factor and minimization of friction and adhesion forces between imprinted features and cavities of the stamp is relevant for upscaling.

Following the strategy described to get high hydrophobic surfaces, the hierarchical structures fabricated in silicon can be optimized by either increasing the depth of the micropillars but keeping a good uniformity of the nanospikes or by increasing the density and shape of nanospikes. Fig. 8(a) describes the density of nanospikes in the hierarchical features studied and these are compared with a non-homogeneous density of nanospikes for higher micropillars (Fig. 8(b)). Finally, Fig. 8(c) describes the shape and density of the nanospikes studied and these are compared with the shape and density obtained in the nanospikes by modifying the plasma treatment protocol (Fig. 8(d)). On the other hand, as mentioned, the imprinted nanospikes are stretched and folded either at the bottom side of micropillars or in the one-layer nanostructures. An optimum demolding protocol to keep the nanospikes standing could lead to that the surface energy released as the cell wall binds to the nanopillar may provide all the energy required to deform the cell wall as it folds around the nanopillar, provoking its stretching, tearing and death. This mechanism, depending on the bacteria's membrane thickness and Young's Modulus was described recently [55]. This bactericidal behavior was not observed as nanospikes were well replicated at top of

the micropillars. It is probably due to either the density of spikes occupies a small part of the total area or that the antimicrobial testing may need more minutes to show it due to bacterial cells may take an active role in binding to the nanospikes, which might yield much higher values of surface energy to deform the membrane in a "slow-binding" approach to nanospikes [55].

Although is difficult to provide general explanation for the attachment of different bacterial species across different surfaces, it is feasible to gain glimpses of the correlations between material chemistry description, topography and wettability properties for individual pathogens associated to its own ability for environmental sensing. To convert these findings into a universal strategy for almost infinite materials and a wide range of topographies with different critical dimensions above and below the bacteria size, the fundamentals of attachment need to be clarified for individual pathogens. This will generate knowledge for intra and interbacterial surface sensing signal transduction mechanisms and establish a suitable protocol for bacteria testing reproducing *in-vitro* what happens in real life conditions. This protocol should be extensible to both hydrophilic and hydrophobic surfaces to avoid false conclusions and consolidate and compare data under the same standard recipe.

4. Conclusions

Passive antibacterial surfaces based on hierarchical features engraved by thermal NIL on PP were fabricated and validated against a Gram-negative (*E. coli*) and Gram-positive (*S. aureus*) bacteria. The introduction of a new approach for evaluating antibacterial performance based on the touch transfer assay was probed to be useful for evaluating highly hydrophobic patterned surfaces and represents an important step towards a unified approach to compare and verify outcomes achieved with new surface treatments and/or patterned surfaces. *E. coli* and *S. aureus* showed to be sensitive to the designed hierarchical features but presented a different behavior. While *S. aureus* was more sensitive to the wettability of the surface, *E. coli* showed an intermediate behavior more closely associated to the topography than to the wettability. Features sizes solely do not seem to have an influence on the surface's antibiofouling properties. This work provides further evidence that cells cannot be treated as inert systems that either attach or not onto a surface as a consequence of a simple interaction between two surfaces of different energies. Instead, signal transduction pathways governed by its own surface appendages and membrane associated sensor proteins play a fundamental role in determining how feasible is for the bacteria to attach depending on wettability, topography and roughness. It means that it constitutes a complex problem in which a library of topographies, surface treatments and materials should be validated against individual pathogens.

This research work constitutes a step towards the high-throughput manufacturing of topography-based surfaces effective against a wide range of pathogens. The fabricated surfaces have shown wear resistance as operating under simulated real environments in hospitals and have been compared to commercial films based on both the use of silver ions

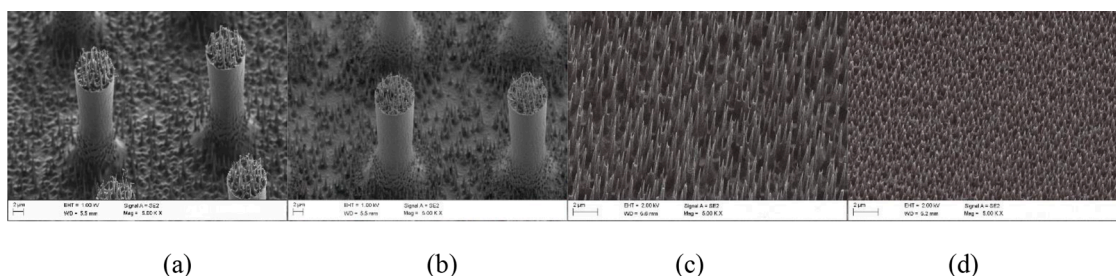


Fig. 8. Further optimization of hierarchical structures fabricated on silicon. (a) Hierarchical structures studied comprised of $10\ \mu\text{m}$ micropillars and nanospikes at the top and the bottom of micropillars, (b) Higher micropillars ($15\ \mu\text{m}$ height) but a lack of uniformity is observed at the bottom, (c) Nanospikes's shape and density studied, (d) The density and shape of the nanospikes can be modified by a modification of the plasma conditions.

or chemical agents and topography. This strategy should be the basis for the fabrication of surfaces fighting concrete pathogens in high demanding sites such as hospitals, outpatient departments, public transport services or used as a consumable for food packaging applications. This strategy avoids or may reduce considerably the use of detergents and chemicals, contributing to avoid pollution and provide environmentally friendly solution, especially when the matrix is substituted by a biodegradable and compostable polymer.

CRedit authorship contribution statement

Achille Francone: Investigation, Writing – original draft, Writing – review & editing. **Santos Merino:** Supervision, Writing – original draft, Writing – review & editing. **Aritz Retolaza:** Writing – review & editing. **Jorge Ramiro:** Writing – review & editing. **Sofia A. Alves:** Writing – review & editing. **Joana Vieira de Castro:** Writing – review & editing. **Nuno M. Neves:** Supervision, Writing – review & editing. **Ainara Arana:** Writing – review & editing. **Jose M. Marimon:** Supervision, Writing – review & editing. **Clivia M. Sotomayor Torres:** Writing – review & editing. **Nikolaos Kehagias:** Supervision, Writing – review & editing.

Declaration of Competing Interest

The authors declare that they have no known competing financial interests or personal relationships that could have appeared to influence the work reported in this paper.

Acknowledgments

This work is funded by the European Commission, under the project FLEXPOL (H2020-NMBPPILOT-2016-721062). The present study was carried out as part of a European project called “Antimicrobial FLEXible POLymers for its use in hospital environments” (FLEXPOL grant agreement No. 721062) funded by Horizon 2020 Framework Programme for Research and Innovation (2014-2020).

References

- [1] Johns Hopkins University of Medicine, COVID-19 dashboard, <https://coronavirus.jhu.edu/map.html>, 2021 (accessed: October, 2021).
- [2] Interagency Coordination Group on Antimicrobial Resistance, Report to the secretary-general of the United Nations (April 2019), https://www.who.int/anti-microbial-resistance/interagency-coordination-group/IACG_final_report_EN.pdf?ua=1, 2021 (accessed: October, 2021).
- [3] Antimicrobial resistance in the age of COVID-19, *Nat. Microbiol.* 5 (2020) 779, <https://doi.org/10.1038/s41564-020-0739-4>.
- [4] World Health Organization. Lack of new antibiotics threatens global efforts to contain drug-resistant infections (January 2020), <https://www.who.int/news-room/detail/17-01-2020-lack-of-new-antibiotics-threatens-global-efforts-to-contain-drug-resistant-infections>, 2021 (accessed: October, 2021).
- [5] A. Bridier, R. Briandet, F. Thomas, F. Dubois-Brissonnet, Resistance of bacterial biofilms to disinfectants: a review, *Biofouling* 27 (9) (2011) 1017–1032, <https://doi.org/10.1080/08927014.2011.626899>.
- [6] M. Cloutier, D. Mantovani, F. Rosei, Antibacterial coatings: challenges, perspectives, and opportunities, *Trends Biotechnol.* 33 (11) (2015) 637–652, <https://doi.org/10.1016/j.tibtech.2015.09.002>.
- [7] C. Mas-Moruno, B. Su, M.J. Dalby, Multifunctional coatings and nanotopographies: toward cell instructive and antibacterial implants, *Adv. Healthcare Mater.* 8 (2019), <https://doi.org/10.1002/adhm.201801103>, 1801103(1)-1801103(26).
- [8] E.P. Ivanova, J. Hasan, H.K. Webb, V.K. Truong, G.S. Watson, J.A. Watson, V. A. Baulin, S. Pogodin, J.Y. Wang, M.J. Tobin, C. L bber, R.J. Crawford, Natural bactericidal surfaces mechanical rupture of *Pseudomonas aeruginosa* cells by cicada wings, *Small* 8 (2012) 2489–2494, <https://doi.org/10.1002/sml.201200528>.
- [9] E.P. Ivanova, J. Hasan, H.K. Webb, G. Gervinskas, S. Juodkakis, V.K. Truong, A.H. F. Wu, R.N. Lamb, V.A. Baulin, G.S. Watson, J.A. Watson, D.E. Mainwaring, R. J. Crawford, Bactericidal activity of black silicon, *Nat. Commun.* 4 (2013), 2838 (1)–2838(7), [10.1038/ncomms3838](https://doi.org/10.1038/ncomms3838).
- [10] A. Morgan, P. Williams, Water contact angle is not a good predictor of biological responses to materials, *Biointerphases* 12 (2) (2017) 02C2011–02C2016, <https://doi.org/10.1116/1.4989843>.
- [11] D. Perera-Costa, J. Morales Bruque, M.L. González-Martín, A.C. Gómez-García, V. Vadillo-Rodríguez, Studying the influence of surface topography on bacterial adhesion using spatially organized microtopographic surface patterns, *Langmuir* 30 (16) (2014) 4633–4641, <https://doi.org/10.1021/la5001057>.
- [12] X. Zhang, L. Wang, E. Levanen, Superhydrophobic surfaces for the reduction of bacterial adhesion, *RSC Adv.* 3 (2013) 12003–12020, <https://doi.org/10.1039/C3RA40497H>.
- [13] T. Ishizaki, N. Saito, O. Takai, Correlation of cell adhesive behaviors on superhydrophobic, superhydrophilic, and micropatterned superhydrophobic/superhydrophilic surfaces to their surface chemistry, *Langmuir* 26 (11) (2010) 8147–8154, <https://doi.org/10.1021/la904447c>.
- [14] X.Q. Dou, D. Zhang, C. Feng, L. Jiang, Bioinspired hierarchical surface structures with tunable wettability for regulating bacteria adhesion surfaces to their surface chemistry, *ACS Nano* 9 (11) (2015) 10664–10672, <https://doi.org/10.1021/acsnano.5b04231>.
- [15] G.B. Hwang, K. Page, A. Patir, S.P. Nair, E. Allan, I.P. Parkin, The anti-biofouling properties of superhydrophobic surfaces are short-lived, *ACS Nano* 12 (6) (2018) 6050–6058, <https://doi.org/10.1021/acsnano.8b02293>.
- [16] A. Jaggesar, H. Shahali, A. Mathew, P.K.D.V. Yarlagadda, Bio-mimicking nano and micro-structured surface fabrication for antibacterial properties in medical implants, *J. Nanobiotechnol.* 15 (64) (2017) 1–20, <https://doi.org/10.1186/s12951-017-0306-1>.
- [17] S.Y. Chou, P.R. Krauss, P.J. Renstrom, Imprint of sub-25 nm vias and trenches in polymers, *Appl. Phys. Lett.* 67 (1995) 3114–3116, <https://doi.org/10.1063/1.114851>.
- [18] H. Schif, Nanoimprint lithography: an old story in modern times? A review, *J. Vac. Sci. Technol. B* 26 (2008) 458–480, <https://doi.org/10.1116/1.2890972>.
- [19] F. Viela, I. Navarro-Baena, J.J. Hernández, M.R. Osorio, I. Rodríguez, Moth eye mimetic cyto-compatible bactericidal nanotopography: a convergent design, *Bioinspir. Biomim.* 13 (2018), <https://doi.org/10.1088/1748-3190/aaa903>, 026011-02625.
- [20] G. Zhang, J. Zhang, G. Xie, Z. Liu, H. Shao, Cicada wings: a stamp from nature for nanoimprint lithography, *Small* 2 (2006) 1440–1443, <https://doi.org/10.1002/sml.200600255>.
- [21] M.N. Dickson, E.I. Liang, L.A. Rodriguez, N. Vollereaux, A.F. Yee, Nanopatterned polymer surfaces with bactericidal properties, *Biointerphases* 10 (2015) 021010–021011, <https://doi.org/10.1116/1.4922157>.
- [22] K. Minoura, M. Yamada, T. Mizoguchi, T. Kaneko, K. Nishiyama, M. Ozminskyj, T. Koshizuka, I. Wada, T. Suzutani, Antibacterial effects of the artificial surface of nanoimprinted moth-eye film, *PLoS One* 12 (2017) 1–19, <https://doi.org/10.1371/journal.pone.0185366>.
- [23] R. Rosenzweig, K. Perinbam, V.K. Ly, S. Ahrar, A. Siryaporn, A.F. Yee, Nanopillared surfaces disrupt *Pseudomonas aeruginosa* mechanoresponsive upstream motility, *ACS Appl. Mater. Interfaces* 11 (2019) 10532–10539, <https://doi.org/10.1021/acsami.8b2226>.
- [24] S. Wu, F. Zuber, K. Maniura-Weber, J. Brugger, Q. Ren, Nanostructured surface topographies have an effect on bactericidal activity, *J. Nanobiotechnol.* 16 (2018) 1–20, <https://doi.org/10.1186/s12951-018-0347-0>.
- [25] F.D. Arisoy, K.W. Kolewe, B. Homyak, I.S. Kurtz, J.D. Schiffman, J.J. Watkins, Bioinspired photocatalytic shark-skin surfaces with antibacterial and antifouling activity via nanoimprint lithography, *ACS Appl. Mater. Interfaces* 10 (23) (2018) 20055–20063, <https://doi.org/10.1021/acsami.8b05066>.
- [26] A. Cumont, R. Zhang, L. Corscadden, J. Pan, Y. Zheng, H. Ye, Antibacterial investigation of a novel coating consisting of mushroom microstructures and HFCD graphite, *Mater. Des.* 189 (2020), <https://doi.org/10.1016/j.matdes.2020.108498>, 108498/1-108498/11).
- [27] A. Fernandez, A. Francone, L.H. Thamdrup, A. Johansson, B. Bilenberg, T. Nielsen, M. Guttman, C.M. Sotomayor-Torres, N. Kehagias, Hierarchical surfaces for enhanced self-cleaning applications, *J. Micromech. Microeng.* 27 (2017), <https://doi.org/10.1088/1361-6439/aa62bb>, 045020/1-045020/9.
- [28] A. Fernandez, A. Francone, L.H. Thamdrup, A. Johansson, B. Bilenberg, T. Nielsen, M. Guttman, C.M. Sotomayor Torres, N. Kehagias, Design of hierarchical surfaces for tuning wetting characteristics, *ACS Appl. Mater. Interfaces* 9 (2017) 7701–7709, <https://doi.org/10.1021/acsami.6b13615>.
- [29] L.R. Bao, X. Cheng, X.D. Huang, L.J. Guo, S.W. Pang, A.F. Yee, Nanoimprinting over topography and multilayer three-dimensional printing, *J. Vac. Sci. Technol. B* 20 (2002) 2881–2886, <https://doi.org/10.1116/1.1526355>.
- [30] F. Zhang, H.Y. Low, Ordered three-dimensional hierarchical nanostructures by nanoimprint lithography, *Nanotechnology* 17 (2006) 1884–1890, <https://doi.org/10.1088/0957-4484/17/8/013>.
- [31] H. Gao, Z. Liua, J. Zhang, G. Zhang, G. Xie, Precise replication of antireflective nanostructures from biotemplates, *Appl. Phys. Lett.* 90 (2007), <https://doi.org/10.1088/0957-4484/17/8/013>, 123115/1-123115/3.
- [32] B. Radha, S.H. Lim, M.S.M. Saifullah, G.U. Kulkarni, Metal hierarchical patterning by direct nanoimprint lithography, *Sci. Rep.* 3 (2013) 1078/1, <https://doi.org/10.1038/srep01078>, 1078/8.
- [33] R.Z. Shafagh, J.X. Shen, S. Youhanna, W. Guo, V.M. Lausckhe, W. Van Der Wijngaart, T. Haraldsson, Facile nanoimprinting of robust high-aspect-ratio nanostructures for human cell biomechanics, *ACS Appl. Bio Mater.* 3 (2020) 8757–8767, <https://doi.org/10.1021/acsbm.0c01087>.
- [34] M.T. Alameda, M.R. Osorio, J.J. Hernández, I. Rodríguez, Multilevel hierarchical topographies by combined photolithography and nanoimprinting processes to create surfaces with controlled wetting, *ACS Appl. Nano Mater.* 2 (2019) 4727–4733, <https://doi.org/10.1021/acsnm.9b00338>.
- [35] E. Psochia, L. Papadopoulos, D.J. Gkiliopoulos, A. Francone, M.E. Grigora, D. Tzetzis, J. Vieira de Castro, N.M. Neves, K.S. Triantafyllidis, C.M. Sotomayor Torres, N. Kehagias, D.N. Bikiaris, Bottom-up development of nanoimprinted plla composite films with enhanced antibacterial properties for smart packaging

- applications, *Macromol* 1 (2021) 49–63, <https://doi.org/10.3390/macromol1010005>.
- [36] M. Nerantzaki, N. Kehagias, A. Francone, A. Fernández, C.M. Sotomayor Torres, R. Papi, T.C. Papadopoulou, Design of a multifunctional nanoengineered PLLA surface by maximizing the synergies between biochemical and surface design bactericidal effects, *ACS Omega* 3 (2018) 1509–1521, <https://doi.org/10.1021/acsomega.7b01756>.
- [37] N. Atthi, O.U. Nimittrakoolchai, S. Supothina, J. Supadech, W. Jeamsakiri, A. Pankiew, C. Hruanun, A. Poyai, An effect of silicon micro-/nano-patterning arrays on superhydrophobic surface, *J. Nanosci. Nanotechnol.* 11 (2011) 8967–8973, <https://doi.org/10.1166/jnn.2011.3505>.
- [38] A.B.D. Cassie, S. Baxter, Wettability of porous surfaces, *Trans. Faraday Soc.* 40 (1944) 546–551, <https://doi.org/10.1039/TF9444000546>.
- [39] R.N. Wenzel, Resistance of solid surfaces to wetting by water, *Ind. Eng. Chem.* 28 (8) (1936) 988–994, <https://doi.org/10.1021/ie50320a024>.
- [40] A. Perez Gavilán, J. Vieira de Castro, A. Arana, S. Merino, A. Retolaza, S.A. Alves, A. Francone, N. Kehagias, C.M. Sotomayor Torres, D. Cocina, R. Mortera, S. Crapanzano, C.J. Pelegrín, M.C. Garrigos, A. Jiménez, B. Galindo, M.C. Araque, D. Dykeman, N.M. Neves, J.M. Marimón, Antimicrobial activity testing methods for hydrophobic patterned surfaces, *Sci. Rep.* 11 (2021) 6675–6684, <https://doi.org/10.1038/s41598-021-85995-9>.
- [41] Sharklet, The technology of sharklet, <https://www.sharklet.com/our-technology/technology-overview/>, 2021 (accessed: October, 2021).
- [42] Autotex, Autotex AM-product data sheet, <http://autotype.macdermid.com/upload/documents/autotex%20am.pdf>, 2021 (accessed: October, 2021).
- [43] Hexis Graphics, Technical data sheet PURZON060B, https://hexis-graphics.com/documents/fichetechnique/document_en/aut_PURZON060B_FTP_anglais.pdf, 2021 (accessed: October, 2021).
- [44] T. Tsukatani, T. Higuchi, H. Suenaga, T. Akao, M. Ishiyama, T. Ezo, K. Matsumoto, Colorimetric microbial viability assay based on reduction of water-soluble tetrazolium salts for antimicrobial susceptibility testing and screening of antimicrobial substances, *Anal. Biochem.* 393 (2009) 117–125, <https://doi.org/10.1016/j.ab.2009.06.026>.
- [45] C. Wiegand, A. Völpel, A. Ewald, M. Remesch, J. Kuever, J. Bauer, Critical physiological factors influencing the outcome of antimicrobial testing according to ISO 22196/JIS Z 2801, *PLoS One* 13 (2018), <https://doi.org/10.1371/journal.pone.0194339> e0194339(1)–e0194339(15).
- [46] A. Klančnik, S. Piskernik, B. Jeršek, S. Smole Možina, Evaluation of diffusion and dilution methods to determine the antibacterial activity of plant extracts, *J. Microbiol. Methods* 81 (2) (2010) 121–126, <https://doi.org/10.1016/j.mimet.2010.02.004>.
- [47] C. Wiegand, M. Abel, P. Ruth, P. Elsner, U.C. Hipler, *In vitro* assessment of the antimicrobial activity of wound dressings: influence of the test method selected and impact of the pH, *J. Mater. Sci. Mater. Med.* 26 (2015) 18/1, <https://doi.org/10.1007/s10856-014-5343-9>, 18/13.
- [48] M.R. Alexander, P. Williams, Water contact angle is not a good predictor of biological responses to materials, *Biointerphases* 12 (2017), 02C201/1–02C201/6, <https://doi.org/10.1116/1.4989843>.
- [49] A.H.A. Lutey, L. Gemini, L. Romoli, G. Lazzini, F. Fuso, M. Faucon, R. Kling, Towards laser-textured antibacterial surfaces, *Sci. Rep.* 8 (2018), 10112/1–10112/10, <https://doi.org/10.1038/s41598-018-28454-2>.
- [50] A.J. McCarthy, J.A. Lindsay, Genetic variation in staphylococcus aureus surface and immune evasion genes is lineage associated: implications for vaccine design and host-pathogen interactions, *BMC Microbiol.* 10 (2010), 173/1–173/15, [10.1186/1471-2180-10-173](https://doi.org/10.1186/1471-2180-10-173).
- [51] N. Epperlein, F. Menzel, K. Scwibbert, R. Koter, J. Bonse, J. Sameith, J. Kruger, J. Toepel, Influence of femtosecond laser produced nanostructures on biofilm growth on steel, *Appl. Surf. Sci.* 418B (2017) 420–424, <https://doi.org/10.1016/j.apsusc.2017.02.174>.
- [52] A. Peter, A.H.A. Lutey, S. Faas, L. Romoli, V. Onuseit, T. Graf, Direct laser interference patterning of stainless steel by ultrashort pulses for antibacterial surfaces, *Opt. Laser Technol.* 123 (2020), <https://doi.org/10.1016/j.optlastec.2019.105954>, 105954/1–105954/10.
- [53] W. Li, E.S. Thian, M. Wang, Z. Wang, L. Ren, Surface design for antibacterial materials: from fundamentals to advanced strategies, *Adv. Sci.* (2021), <https://doi.org/10.1002/advs.202100368>, 2100368/1–2100368/23.
- [54] T.J. Silhavy, D. Kahne, S. Walker, The bacterial cell envelope, *Cold Spring Harb. Perspect. Biol.* 2 (2010), <https://doi.org/10.1101/cshperspect.a000414> a000414/1–a000414/16.
- [55] G.S. Watson, D.W. Green, J.A. Watson, Z. Zhou, X. Li, G.S.P. Cheung, M. Gellender, A simple model for binding and rupture of bacterial cells on nanopillar surfaces, *Adv. Mater. Interfaces* (2019), <https://doi.org/10.1002/admi.201801646>, 1801646/1–1801646/8.